Using Markov Chain Monte Carlo to Estimate Bearing Condition

H.J. Lawrence, T.C.A. Molteno and C. Fox
Elec Research, Department of Physics
University of Otago.
Email: hilary@elec.ac.nz

***Abstract*—This paper discusses Monte Carlo Markov chain (MCMC) as a tool for the analysis of bearing condition, using vibration data from new and damaged bearings. Analysis done using traditional time-domain and frequency-domain methods indicates vibration signals can be used to estimate bearing condition, but these methods give no information on the certainty of such results. MCMC outputs give the probability distribution of parameters – such as impulse frequency – so not only can this frequency be estimated, but the accuracy of this estimate can also be measured. Using data in the time-domain in MCMCs has some advantages over frequency-domain analysis when separating the individual sources of periodic vibrations.**

I. Introduction

Rolling element bearings are widely used in rotating machinery [1], with single row deep groove ball bearings being the most widely used type [2]. It is useful to monitor the condition of bearings as bearing failure can be expensive, both in terms of damaged machinery and lost production time [3].

In this paper we discuss the use of model based inference, using Markov chain Monte Carlo (MCMC), as a method of vibration analysis of deep groove ball bearings. Experimental work involved periodically measuring vibrations from bearings which have been run from new. This is compared to vibrations from other bearings which have had defects seeded on their races or balls. Initial analysis employed commonly used measures of bearing condition, and results were compared with the physical state of bearings, which was found by cutting them open.

An investigation was done to see if bearing condition can be inferred from vibration data using MCMC and established models of bearing behaviour. In particular, the investigation asked does MCMC perform better than conventional methods of analysis? Are issues faced due to limitations of models, problems with data, or issues with the implementation of MCMC?

This paper includes discussion on the signals used in MCMCs, both synthetic and actual. These signals relate to a mechanical system, and signal voltage is proportional to acceleration at the sensor surface. The versatility of this method means it could be applied to other signal sources using an appropriate model.

II. Model Based Inference and MCMC

A model of any physical system, A, can be used as a forward map [4],

$$A : x \mapsto y, \tag{1}$$

that maps the true state of a system, x, to data from that system, y. The solution to an inverse problem is to attempt to reconstruct the true state of the system from the data, using [4]

$$y = A(x) + \mathbb{N}(0, \sigma), \tag{2}$$

where $A(x)$ is the action of the model on the system, and $\mathbb{N}(0, \sigma)$ is some additive random noise with zero-mean and standard deviation σ. MCMCs are a group of methods that can give solutions to inverse problems, even when they are ill-posed – that is even if there is a range of possible model predictions that fit the data [4].

A. Adaptive Metropolis-Hastings

A Markov chain involves the drawing of random variables from a state space, Ω, in order to estimate the target distribution. A state space may be discrete or continuous, and contains all allowed states of the parameters that describe the model. Each new drawing of a random variable depends only on the previous value, and does not depend on any values drawn before that. This is known as the Markov condition [5]. See Gamerman [5] for more on the properties of a Markov Chain.

The random walk Metropolis-Hastings (MH) is a method of generating a Markov chain that converge on the equilibrium distribution as the length of the chain becomes large [6]. The random walk begins in some prior state $\mathbf{X_n} = \mathbf{i}$, drawn from Ω. A new state is proposed by making a random step from this state. Steps used in these MCMCs have the form

$$\mathbf{j} = \mathbf{i} + \mathbb{N}(\mathbf{0}, \mathbf{C}), \tag{3}$$

where C is the proposal covariance. This new proposal is then accepted or rejected according to the acceptance probability $\alpha(j \mid i)$. This can be expressed in terms of the Hastings ratio, which for a symmetric proposal is [6]

$$\alpha(j \mid i) = \min\left\{1, \frac{Pr(j \mid y)}{Pr(i \mid y)}\right\}, \tag{4}$$

where $Pr(j \mid y)$ and $Pr(i \mid y)$ are the probability of the j^{th} and i^{th} states, given the data y. $Pr(j \mid y)$ is calculated using

Bayes Theorem, and in the unnormalised case this is given by [4]

$$Pr(j \mid y) \propto Pr(y \mid j)Pr(j), \tag{5}$$

where $Pr(y \mid j)$ is the likelihood, and $Pr(j)$ is the prior distribution of j. If accepted, $\mathbf{X_{n+1}} = \mathbf{j}$, and if rejected $\mathbf{X_{n+1}} = \mathbf{i}$. The next proposed state is a random walk from $\mathbf{X_{n+1}}$. The Metropolis-Hastings algorithm can be applied to a multi-dimensional distribution by proposing a change to all variables at once, or by changing only one variable during each proposal.

The adaptive Metropolis (AM) algorithm allows the proposal covariance to be periodically updated from some initial estimate, C_o, using the covariance of the Markov chain, Σ [6], [7]. At chain iteration t the proposal covariance is given by [7]

$$C_t = \begin{cases} C_o & t \leq t_o \\ \frac{\phi^2}{d}\Sigma_{t-1} + \frac{\phi^2}{d}\varepsilon\mathbf{I} & t > t_o, \end{cases} \tag{6}$$

where t_o is the initial non-updating period, ϕ is a scaling value, d is the number of dimensions in Ω, $\mathbf{I}$ is a $d \times d$ Identity Matrix, and ε is a small positive constant, chosen empirically to prevent the chain becoming stuck. See Haario and references therein [7] for more on AM, including the choice of ϕ and ε.

III. Gathering the Bearing Dataset

The experiment set-up is shown in Figure 1. An Associated Electrical Industries AC motor is used to drive a shaft which is held in place by two 6204.2 single row ball bearings – the 'experiment bearing' is housed furthest from the motor. A third 6006.2 bearing is used as part of the load set-up. Experiment control is provided by a Xilinx Spartan-3 FPGA, using inputs from an HEDS-9140 shaft encoder. Vibrations were detected with a Brüel & Kjær accelerometer of type 4519-002, with sensitivity of 10mV/g (where g $= 9.81\text{ms}^{-2}$), attached to the side of the bearing housing. Data logging was done using a National Instruments ELVIS Development Board, connected to a PC running National Instruments SignalExpress.

Thirty-one bearings were run in the "experiment bearing" position. These are labeled in sets, according to defect type (or lack of defect), as UD1-10, ID1-8, OD1-7 and BD1-6, where UD=undamaged, ID=inner race defect, OD=outer race defect and BD=ball defect. UD1-10 were run for 56 hours, with data logged once per hour for 20 s. The other 21 bearings were run in for 18.5 hours prior to the seeding of defects. A single seeded defect was applied to each bearing according to the labels above. A second defect was seeded on each of OD7 (ball), ID7 (ball) and ID8 (outer race). Bearings were run for a further 36 mins, and data were gathered for 60 s at 25, 30 and 35 mins.

A range of defect sizes were seeded, and analysis of the resulting signal in the time-domain indicated that vibrations from some bearings were difficult to distinguish from those from UD1-10, while others were clearly different. When defect sizes were divided into "larger" and "smaller" categories there was good agreement between vibration amplitudes and defect sizes, but within each category correlation was less clear. Reasons for this include variations in the state of bearings before defects were seeded, balls also being damaged slightly during the seeding of race defect, and defects of different types

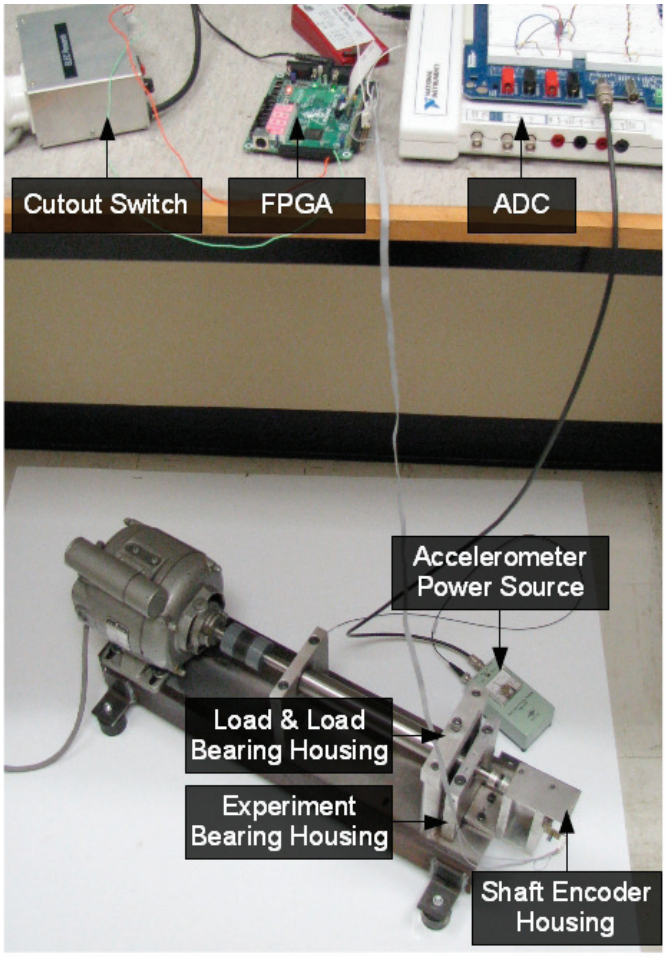

Fig. 1. Experimental setup used in all experiments.

effecting vibrations in different ways – this is due in part to differences in geometry between the inner and outer races [3]. In the case of ball defects, the contact time between defect(s) and races vary with the orientation of the ball [8].

IV. Adaptive Metropolis for Bearing Analysis

AMs were run on selected data from each bearing, with each data used in 2-4 separate MCMCs. A synthetic signal is created during each iteration of the AM, with properties that depend on the current state of model parameters. This is compared with the bearing data, in order to create an empirical likelihood function, $L(y \mid x_S)$, which allows $Pr(j \mid y)$ to be estimated using Equation 5. Uniform priors are used in this investigation. Gaussian priors - selected in part from the outcome of this investigation – are used in later MCMCs.

A. The Model

The bearing-race system can be modeled as a spring-damper system [9], [10]. The mass and stiffness of the races and rolling elements, as well as damping provided by lubrication can be used to predict how the ball and races will flex during bearing motion. Models predict that even an undamaged bearing will generate periodic impulses as contact forces vary when the balls rotate [11]. The outer [10] (or both [8]) races

can be modeled to flex at their natural frequency, causing resonance triggered by these periodic impulses. In addition, when a bearing is damaged additional impulses are predicted, and these also trigger resonance [12].

If it is assumed that there is no slippage between the rolling elements and the races, then the geometry of the bearing determines the impulse frequencies. It is common practice to relate other frequencies to the shaft frequency, f_s, the diameter of the rolling elements, d, the cage diameter, D, and the contact angle α [1], [8], [11]. Of interest in this investigation are the cage rotation frequency (f_c), the ball pass frequency (f_{bps}) – this is the frequency at which balls pass a fixed point, such as the point of maximum load – and the defect frequencies. The defect frequencies describe the rate at which balls impact with a defect on the outer race (f_{od}) or the inner race (f_{id}), or the rate a defective ball impacts with either race (f_{bd}). Note that $f_{bps} = f_{od}$ for a bearing with a stationary outer race. Even undamaged bearings are predicted to have impulses at f_{bps}, and f_{bps} is used as the reference frequency in MCMCs rather than f_s.

We assume a simplified model with four sources of periodic impulses that trigger flexural vibrations at the natural frequencies of the outer race. Each source is assumed to create a damped periodic response. The sources, along with the prior assumption of their frequency, are:

1) Balls passing in and out of the load zone (f_{bps}).
2) Balls passing a small defect or surface imperfection on the outer race (f_{od}).
3) Impacts between races and a small defect or surface imperfections on a single ball (f_{bd}).
4) Balls passing a small defect or surface imperfections on the inner race (f_{id}).

The four resulting impulses each have a periodicity ($f_{Iz}, z \in 1...4$), which may modulate by some amount (M_z), at some frequency (f_{mz}). Impulses also have an amplitude (A_z), and a pulse decay constant (τ_z). Sources 1 and 2 are at the same frequency (i.e. $f_{I1} = f_{I2}$), and have a phase relationship ($\phi_{1,2}$). The noise term (effectively the sum of all other vibration) can be modeled as Gaussian noise by the central limit theorem [13], with $\mathbb{N}(0, \sigma_N)$, where σ_N is a dimension in Ω. This creates a 19 parameters in Ω, as source 1 is assumed to have no modulation.

B. Estimating Likelihood

The envelope method is a widely used method of recovering the frequencies discussed in Section IV-A [1], [3], particularly the defect frequencies [12]. A signal $x(t)$ is bandpass filtered around a structural resonance frequency. The filtered signal $x_f(t)$ is demodulated by taking the envelope, using the Hilbert transform [11]. This leads to the instantaneous amplitude $\mid y(t) \mid$, or envelope, of the filtered signal

$$\mid y(t) \mid \;=\; \sqrt{x_f(t)^2 + \mathcal{H}(x_f(t))^2}, \qquad (7)$$

where $\mathcal{H}(x_f(t))^2$ is the Hilbert transform of $x_f(t)$.

The final stage of the envelope method, as it is used in signal processing, is to take the Fourier transform of the envelope in order to recover the frequency of any repeating

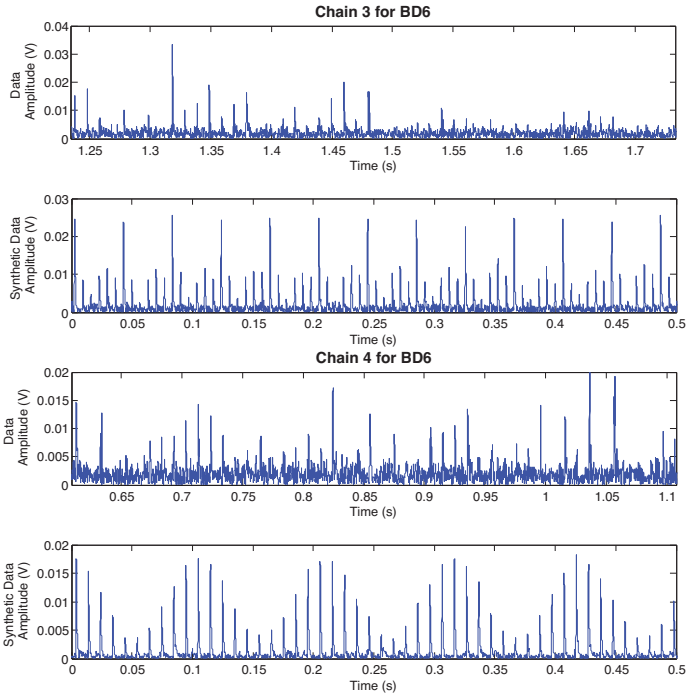

Fig. 2. Comparison between data from BD6 (with a defect on a ball) and synthetic signals from two MCMCs from the chain state corresponding to the maximum log-likelihood for each. The first 0.5 s (of 1 s) of the portion of data where the highest correction with the synthetic signal occurs is shown for each. Chain 3 produces a lower posterior distribution for log-likelihood than Chain 4, as the MCMC has become stuck at a local maxima.

periodic impulses [11]. When using this method it is not possible to separate multiple sources that cause spectral peaks at the same or similar frequencies without the further preprocessing of data. Other methods of filtering and/ or preprocessing in the frequency-domain, or analysis in the time-frequency domain, can provide better resolution for particular data. The envelope method (with selected filter) was found to be the best performing overall for bearings in any condition, as well as taking less processing time than many other methods.

The (enveloped) data $y(t)$ is created by taking 3.33 s of data from a selected bearing, and applying the envelope method, after filtering around the $n = 3$ mode of flexural vibration of the outer race. The synthetic data is filtered in the same manner as the bearing data, to create the synthetic envelope data $x_S(t)$ with length 1 s. The data and synthetic signal remain in the time-domain. Figure 2 gives two examples of synthetic signals created during the running of MCMCs using data from BD6 (also plotted). These are discussed further in Section VI.

The Matlab [14] function xcorr is used to create the normalised correlation, $R(\tau)$, between the synthetic and actual data, considering only the portion of the correlation that corresponds to $x_S(t)$ being fully overlapped with $y(t)$. The maximum normalised correlation, $R(\tau_{max}) = \sup(R(\tau))$ is used in the calculation of $L(y \mid x_S)$.

Early trials of MCMCs indicated that impulse amplitudes, A_z, need to be limited, so an amplitude scaling term is

introduced to achieve this:

$$A_S = \frac{V_{rms}(x_S)}{V_{rms}(y_{\tau_{max}})}, \quad (8)$$

where $V_{rms}(y_{\tau_{max}})$ is the root mean square voltage of the section of $y(t)$ corresponding to $R(\tau_{max})$.

A weighting term $W = 30$ is included in the empirical likelihood giving

$$L(y \mid x_S) \propto exp\Big\{ -W\big(1 - R(\tau_{max})\big) - \big(A_S - 1\big)^2 \Big\}. \quad (9)$$

The $1-R(\tau_{max})$ term is required for the acceptance probability to increase as $R(\tau_{max})$ gets larger.

C. Updating the Proposal Covariance

The proposal covariance was updated using Equation 6. Using $\phi = 2.4$ is found to optimise mixing [7], [15]. In addition, $\varepsilon = 10^{-5}$ [16] and the number of dimensions, $d = 19$, were used giving

$$C_t = \frac{2.4^2}{19}\Sigma_{t-1} + \frac{2.4^2}{19}(10^{-5})\mathbf{I}. \quad (10)$$

The initial covariance was based on one used by Cui [6], where $C_o = \frac{0.1^2}{d}\mathbf{I}$. All MCMCs used an initial non-updating period of $t_o = 100$ samples, and C_t was updated every 100 samples from 100-20,000 samples. This was continued for the entire chain (300,000 samples) for some MCMCs, and in others C_t was updated every 300 samples from 20,000-300,000 samples. There was found to be no noticeable difference between these options, and updating every 100 samples for the entire MCMC became the default choice. Updating C_t more often reduced the performance of chains, as occasional large transitions had too great an effect on the covariance early in an MCMC. This is consistent with Haario, who found that updating the covariance every step was not useful [7].

V. Results

In most bearings 1-2 sources dominated, and produced useful posterior distributions. Other source(s) from each bearing produce wide posterior marginal distributions for parameters relating to frequency and posterior marginal distributions for amplitude and pulse width with modes at (or close to) zero. The assumed mapping of impulses to sources was not reflected in all posterior distributions. This is discussed further in Section VI. Sections V-A – V-C briefly discuss a selection of MCMC outputs, showing the behaviour of different parameters.

A. Bearings with Outer Race or No Defects

Bearing models predict that impulses at f_{bps} should not be modulated except in the case of an unbalanced shaft [9] or cage [11]. These MCMCs tested this assumption by setting $M_1 = 0$. Many of UD1-10 instead mapped impulse 2, with $M_2 \neq 0$, to source 1 (balls passing the load). Figure 3 shows outputs from UD3 and UD5. Note that M_2 is indicated by colour temperature. UD5 in particular has a narrow (but multi-modal) joint posterior distribution for f_{I2} vs f_{m2} vs M_2 that indicates high modulation at frequencies that relate to combinations of f_s and f_c. These are predicted in the case of shaft imbalance

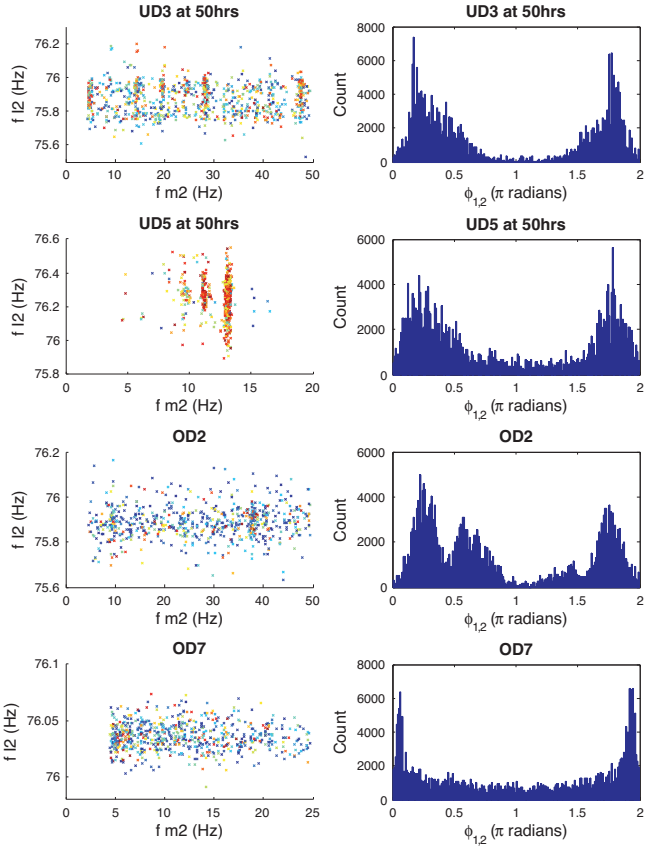

Fig. 3. Joint posterior distribution of f_{I2} vs f_{m2} vs M_2 and marginal distribution for $\phi_{1,2}$ for UD3 and UD5 at 50 hours and OD2 and OD7 after the application of seeded defects to the outer race. M_2 is indicated by colour temperature. Note that f_{I2} is centred around similar values for all bearings, but f_m and $\phi_{1,2}$ vary between undamaged bearings and those with defects on the outer race.

[11]. The outputs for f_{m2} are quite different for UD3 and UD5 (and others of UD1-10) indicating that small changes in operating conditions significantly effect this parameter.

UD1-10 all produce similar posterior marginal distributions for $\phi_{1,2}$. These suggest a single vibration source with multiple impulses per period, which is supported by the load zone model. A version of the model that builds these features into source 1 is being trialled. This updated model uses Gaussian priors for all non-zero f_{Iz} and f_{mz} parameters, including a prior of $\mathbb{N}(\frac{1}{2}f_s, 5)$ Hz for f_{m1} ($\frac{1}{2}f_s \approx 12.4$ Hz).

Signal processing in the frequency domain indicates that it can be difficult to distinguish between impulses from undamaged bearings and those with outer race defects. The posterior marginal distribution for $\phi_{1,2}$ for OD2 is multi-modal. There are modes that are similar to the modes from UD3 and UD5 (and other undamaged bearings), and in addition, there is another mode at about 0.6π rad (and a smaller one at about 1.4π rad). An interpretation of this is that the 0.6π rad mode relates to the relative positions of the load and the defect. Outputs from OD7 indicate it has a single source with $f_{I2} \approx f_{od}$. Each MCMC produces modes of $\phi_{1,2}$ that are close to 0 (or 2π) radians, suggesting that the rectangular defect coincides with the position of the centre of the load zone, or

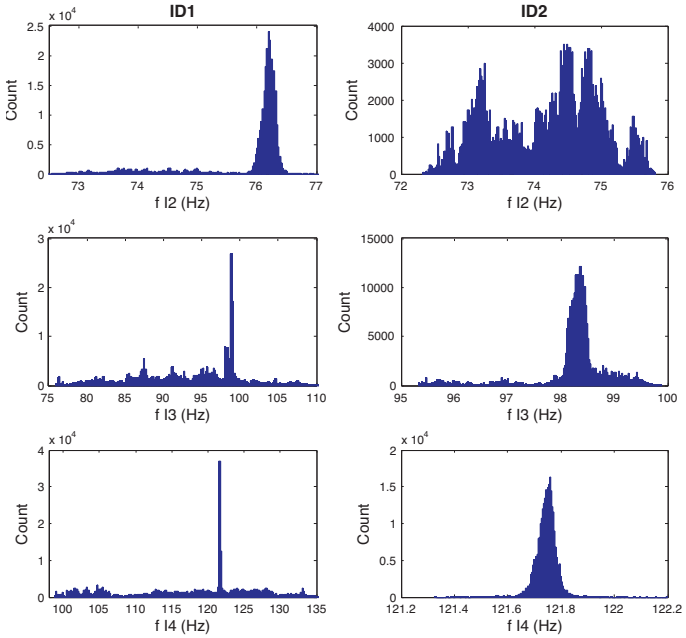

Fig. 4. Marginal posterior distributions for f_{I1}, f_{I3} and f_{I4} for ID1 and ID2. Each has a seeded defect on the inner race, and a damaged ball. Both bearings have modes at approximately f_{bd} and f_{id}, with the narrowest distribution coming from the short, deep, inner race defect on ID2.

that impulses due to the defect dominates other vibrations. Note also that OD2 and OD7 have low modulation. OD6 (see Figure 5) does have modulation at $\frac{1}{2}f_{od}$, but this frequency is not highly probable in outputs from UD1-10 (or OD6 pre-defect).

B. Bearings with Multiple Sources

Figure 4 shows the posterior distribution for all impulse periodicities for ID1-2 (note that $f_{I1} = f_{I2}$). These bearings have multiple impulse sources, as in addition to the inner race defects, each bearing had balls damaged during the defect seeding process. This was noted during signal processing, however the sideband frequency due to a moving inner race defect is at a similar value to the ball defect frequency (i.e. $f_{id} - f_s \approx f_{bd}$), so these sources were not well resolved in the frequency domain. ID1 has wide distributions, with clear modes at f_{bps}, f_{bd} and f_{id}. At any particular chain iteration, the MCMC is sampling near 1-2 of these modes.

ID2 has a narrow distribution for f_{I4}, with $\bar{f_{I4}} \approx f_{id}$. Bearings with short, deep, defects (such as ID2) tend to produce narrower distributions at the relevant defect frequency than those with longer defects (such as ID1). The middle plot for ID2 has a clear mode near to f_{bd}, but the top plot shows no clear mode near f_{bps}. This inability to find the periodicity at f_{bps} also occurs in other bearings with significant defects, and may be due to this impulse being obscured by other vibrations [3].

C. Amplitude and Impulse Width

Figure 5 shows outputs relating to the largest impulse for four bearings. Colour temperature indicates modulation depth

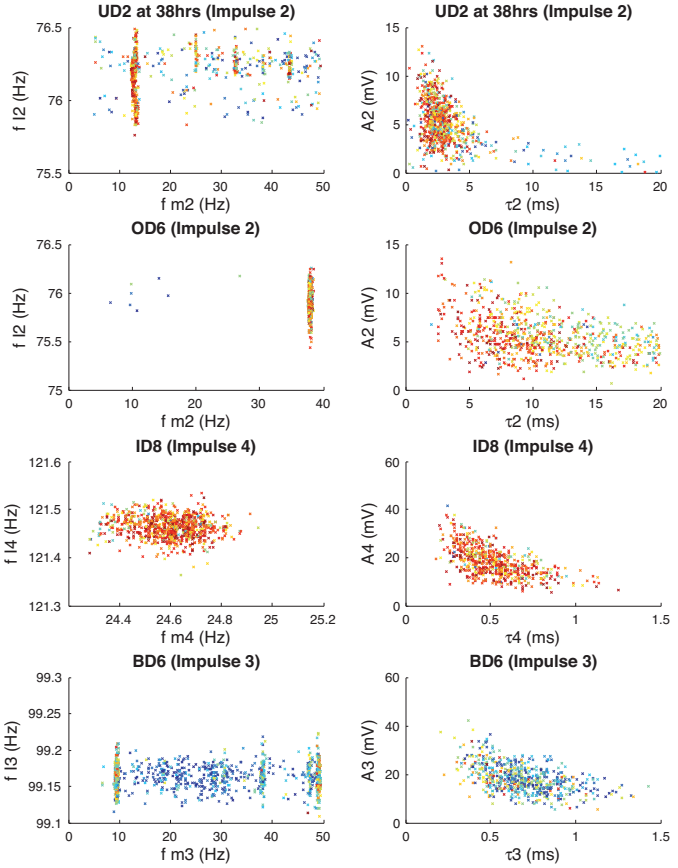

Fig. 5. Joint posterior distributions for f_{Ix} vs f_{mx} vs M_x and A_x vs τ_x vs M_x, for UD2 at 38 hours ($x = 2$), and OD6 ($x = 2$), ID8 ($x = 4$) and BD6 ($x = 3$) after the application of seeded defects. M_x is indicated by colour temperature, and these bearings all have evidence of moderate-high modulation, with that from ID8 and BD6 being due to defects moving in and out of the load zone [12].

M. UD2 is plotted as it has one of the highest amplitudes at f_{bps} of any of UD1-10. The amplitude of OD6 is similar, but the pulse width (τ_2) indicates a high probability of a much longer impulse than any from UD1-10 (or most other bearings). Outputs from all of OD1-7 indicate a relationship between defect length and the posterior distribution of τ_2. This does not occur for inner race defects or most ball defects, which produce posterior distributions for τ similar to those shown in Figure 5 for ID8 and BD6, irrespective of defect size. This is consistent with findings from Al-Dossary [17], who found a relationship between defect size and acoustic burst duration for outer race defects, but not for inner race defects. The model assumes that flexing of the outer race is the main contribution to a bearing's vibrations over the frequency band used. For defects other than those on the outer race, it appears that impulses are due to a single event – for example the initial impact with a defect. One of the limitations of this model is that the impacts between a ball defect and each race are assumed to have the same properties, which may not be the case.

D. Frequencies of Interest

Discrepancies between measured and predicted values of the frequencies of interest were noted during signal processing

– these were investigated further using MCMC outputs. Figure 5 shows the marginal distribution for impulse 4 from ID8 – this has narrow distributions for $f_{I4} \approx f_{id}$ and $f_{m4} \approx f_s$. Another MCMC from ID8, and two for ID2 had similar narrow distributions. These outputs were used to make re-estimates of the effective values of d, D, and α. This led to re-estimates of the frequencies of interest, which were compared to relevant posterior marginal distributions from other bearings. These results suggest that race misalignment ($\alpha \neq 0$) is the physical cause of some, but not all, of this discrepancy. Other contributions could be due to changes in the effective value of bearings dimensions during the operation of the bearing. When trying to make such re-estimates using data in the frequency-domain or time-frequency domain, and traditional signal processing methods, there are limitations. When using the envelope method, these limitations include FFT bin width and peaks being averaged over the length of data. In addition it is difficult to map spectral peaks to individual impulse source(s), and measurement uncertainty cannot be estimated.

VI. Discussion and Conclusion

This investigation indicated that MCMC is potentially a useful tool in analysing a vibration data, but there are still issues that need to be resolved. These include long running times (in the order of hours), limitations in the model and some problems with the method of calculating the empirical likelihood function. Some MCMCs (18 out of 185 run) became stuck at local maxima, where the synthetic signal had a reasonable correlation with large peaks, but other peaks did not correlate well. In some instances this occurred when the impulse was at a sideband frequency, and modulation was at the difference frequency. For example, chain 3 from BD6 has $f_{I2} \approx f_{bd} - f_s$, and $f_{m2} \approx f_s$, and a lower empirical likelihood (and lower correlation) than other MCMCs (chains 1,2,4) run from this data. Figure 2 shows a single synthetic signal from each of chains 3 and 4. Also plotted is the portion of $y(t)$ that corresponds with the maximum correlation ($R(\tau_{max})$). Chain 4 plots show a reasonable correlation between both larger and smaller peaks.

Other issues faced included impulses not matching to sources as defined in Section IV-A – so different MCMCs run using the same data could not be easily combined. Some outputs from bearings with seeded defects were difficult to distinguish from UD1-10, but in all but one case these were from bearings with only slight defects. Bearings with longer defects on the inner race did not match the model well, but most produced outputs that were different from UD1-10.

UD1-10 produced similar outputs from most MCMCs, with some indication of variations relating to imbalance in the shaft or cage of some of these bearings. Bearings with seeded defects produced MCMC outputs that differed from undamaged bearings in most cases. Bearings with shorter, deeper defects fitted the model best and in some cases multiple defect sources could be well resolved. These results led to proposed adjustments to the model, including the introduction of Gaussian prior distributions for some parameters.

The advantage of MCMC is that a probability distribution is associated with each output, and poorly known parameters have wide or multi-modal distributions. In addition, by using data in the time domain, the sources of different spectral peaks in the frequency domain could be separated. This separation allowed some investigation into discrepancies between predicted and actual values of frequencies of interest, including those relating to impacts with defects.

References

[1] N. Tandon and A. Choudhury, "A review of vibration and acoustic measurement methods for the detection of defects in rolling element bearings," *Tribology International*, vol. 32, pp. 469–480, 1999.

[2] NSK, *Rolling Bearings Catalog (CAT No E1102i)*, ©NSK Ltd, http://www.nsk.com, 2005.

[3] X. Williams and T. Ribadeneira, "Rolling element bearing diagnostics in run-to-failure lifetime testing," *Mechanical Systems and Signal Processing*, vol. 15, no. 5, pp. 979–993, 2001.

[4] T. Cui, C. Fox, and M. J. O'Sullivan, "Bayesian calibration of a large-scale geothermal reservoir model by a new adaptive delayed acceptance Metropolis Hastings algorithm," *Water Resources Research*, vol. 47, no. 10, 2011.

[5] D. Gamerman, *Markov Chain Monte Carlo*. Chapman & Hall, 1997.

[6] T. Cui, "Bayesian Calibration of Geothermal Reservoir Models via Markov Chain Monte Carlo," *University of Auckland*, 2010.

[7] H. Haario, M. Laine, A. Mira, and E. Saksman, "DRAM: Efficient adaptive MCMC," *Statistics and Computing*, vol. 16, no. 4, pp. 339–354, Dec. 2006.

[8] S. Sassi, B. Badri, and M. Thomas, "A Numerical Model to Predict Damaged Bearing Vibrations," *Journal of Vibration and Control*, vol. 13, no. 11, pp. 1603–1628, 2007. [Online]. Available: http://jvc.sagepub.com/content/13/11/1603

[9] S. Harsha, K. Sandeep, and R. Prakash, "The effect of speed of balanced rotor on nonlinear vibrations associated with ball bearings," *International Journal of Mechanical Sciences*, vol. 45, pp. 725–740, 2003.

[10] J. Wensing, "On the dynamics of ball bearings," *University of Twente*, December 1998.

[11] Z. Karagulle and H. Kiral, "Simulation and analysis of vibration signals generated by rolling element bearing with defects," *Tribology International*, vol. 36, pp. 667,678, September 2003.

[12] P. McFadden and J. Smith, "Model for the Vibration Produced by a Single Point Defect in a Rolling Element Bearing," *Journal of Sound and Vibration*, vol. 96, no. 1, pp. 69–82, 1984.

[13] J. Jiang and B. Zhang, "Rolling element bearing vibration modeling with applications to health monitoring," *Journal of Vibration and Control*, vol. 18, no. 12, pp. 1768–1776, 2012.

[14] MATLAB, *Version 7.11.0.584 (R2010b)*, ser. . Natick, Massachusetts: ©The MathWorks Inc., 1984-2010.

[15] A. Gelman, G. Roberts, and W. Gilks, "Efficient Metropolis Jumping Rules," *Bayesian Statistics*, vol. 5, pp. 599–607, 1996.

[16] M. Laine, *DRAM - Delayed Rejection Adaptive Metropolis*, www.helios.fmi.fi/ lainema/dram/.

[17] S. Al-Dossary, R. Hamzah, and D. Mba, "Observations of changes in acoustic emission waveform for varying seeded defect sizes in a rolling element bearing." *Applied Acoustics*, vol. 70, no. 1, pp. 58–81, January 2009.